

In-situ

K C , W , L ,*, L H , C , L , f L ,
s W , K s Ess , L L , G , T P J^f



Gemological Institute, China University of Geosciences, Wuhan 430074, PR China
 Hubei Gem and Jewelry Engineering Technology Research Center, Wuhan 430074, PR China
 School of Materials Science and Engineering, Huazhong University of Science and Technology, Wuhan 430074, PR China
 Mechanical Engineering, University of Birmingham, Birmingham B15 2TT, UK
 School of Electrical and Electronic Engineering, Huazhong University of Science and Technology, Wuhan 430074, PR China
^fWMG, Materials Engineering Centre, University of Warwick, CV4 7AL Coventry, UK

ARTICLE INFO

Keywords:

T - s s l
 C s s ff l
 S l l s l
 C l s
 El f s l

ABSTRACT

C l , - s l (3DG) f s s l ss, s
 l s s ll s s l . H s l - s l -
 s s l l s l (SLM) f - s l (3D) s C
 l . G s in-situ l s (CVD) s C
 l , f 3DG s s . A f l CVD
 SLM f s ff l l s l f 3DG f -s ()
 , s ,) -s (X , s f l) s
 s ff l . T 3DG/ s ff l l 88% 27% l
 f (EMI) s l ff s X s l . P SE f 32.3 B s EMI s l ffi-
 (SE) 47.8 B 2.7 GH X SE f 32.3 B f 2-18 GH .
 T s s s l s s f f s f s
 l s s f SLM s s .

1. Introduction

G , s s f sp^2 s, s
 s f (2630 2^{-1}) 1, X ll s f , s s
 (2 10^5 2^{-1} V^{-1} s^{-1}) s l
 (615000 $W^{-1} K^{-1}$) 2 . H , s π - π
 s l (2D) s l - s s -
 ll, s ll, l, f l - l ss s s s l s f l l
 3 . Af f s l s fi l ff s s
 l s . C f s l s, - s l - s s l s
 (3DG) s s s (99.7%), l s , l l - CVD s s s s , s
 s fi (0.6 $^{-2}$) 4 s fi ll s s f l - l 16 . B
 s f s s ll s l , f s l s , f s l , s s l l
 ss sf s f - s l f l s s s s

*C s : G l l I s , C U s f G s s, W 430074, PR C .
 E-mail address: l@ . . (. L).

l s . T X s s s (. . , s -
s) , X fl fi l s -
(. . , l ss, f s) f 3DG. B s s, -
(. . , s , s , s f l). H , s f l s -
l l s s , f s , l N f -
l l s s l l f -
s s s l 3DG s s l f -
s s s f s f s fi f l s 17,18 .
H , s f ss l l l s, -
s l l f s s 3DG -
l s s s l f s 19 .
S l l s l (SLM), s -
f (AM) l , s l l s f f -
f s s / s X - s l (3D) l l s -
fi X l f in-situ f l . T , s -
s s SLM s s s f T l l s 20 ,
s l ss l l s 21 , N l l s 22 . C s s l s f l /
s s f l - s s s - f - -
s s l s . C N s s ,
s s s l s s f -
CVD l s l (< 0.001 . %) -
l s l l f , s 23 . W l N s -
l s l l (> 0.1 . %) 17 , fi l s -
f s f X ss 24 . H , -
s SLM f s s l l s f s ffi -
f s l f s s s l l -
fl s l s l -
(1000-1100) . F f s s s ff l s -
SLM s s l l f l l s 25 .
T l l s, f fi s s -
f s l - 3DG/ (3DG/C) s -
s SLM s l s l CVD f -
l . A l l - s s l l s -
l l s SLM f s l l -

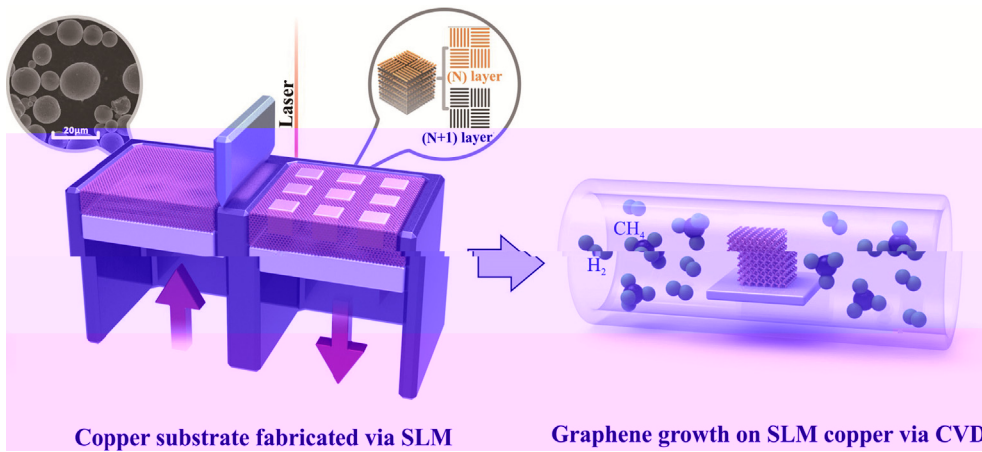


Fig. 1. SLM of copper substrate and in-situ CVD growth of graphene on SLM copper substrate.

ASTM B193-2002 (2010) and ASTM E1461-2013 (2013) for mechanical testing. The tensile test was performed using a universal testing machine (LFA457, Instron) with a load cell of 5 kg. The test specimens were prepared according to the standard. The microstructure was analyzed using a scanning electron microscope (SEM, JEOL JSM-7000F) and an energy-dispersive X-ray (EDS) spectrometer. The Raman spectra were recorded using a Renishaw inVia Raman microscope with a 532 nm laser source. The laser power was 400 mW and the spot size was 130 μm. The scanning rate was 1800 cm⁻¹ min⁻¹. The Raman spectra were fitted with Origin software. The G and 2D bands were deconvoluted into three Lorentzian peaks. The intensity ratio of the G and 2D bands (I_G/I_{2D}) was used to evaluate the defect density of the graphene. The surface morphology was characterized by atomic force microscopy (AFM, Bruker MultiMode 8) in air. The surface area was calculated using the AFM images. The surface energy was calculated using the contact angle measurements. The contact angle was measured using a contact angle goniometer (OCA 20, DataPhysics Instruments) with distilled water as the probe liquid. The surface energy was calculated using the Young's equation. The surface energy was 28.5 mJ m⁻².

3. Results and discussion

3.1. Formation of SLM copper

3.1.1. SLM manufacturing of copper under different line energy densities

The SLM process parameters were varied to study the effect of line energy density on the microstructure and mechanical properties of the SLM copper. The line energy density was defined as the laser power divided by the scanning speed. The SLM copper was fabricated under different line energy densities, as shown in Fig. 2(a).

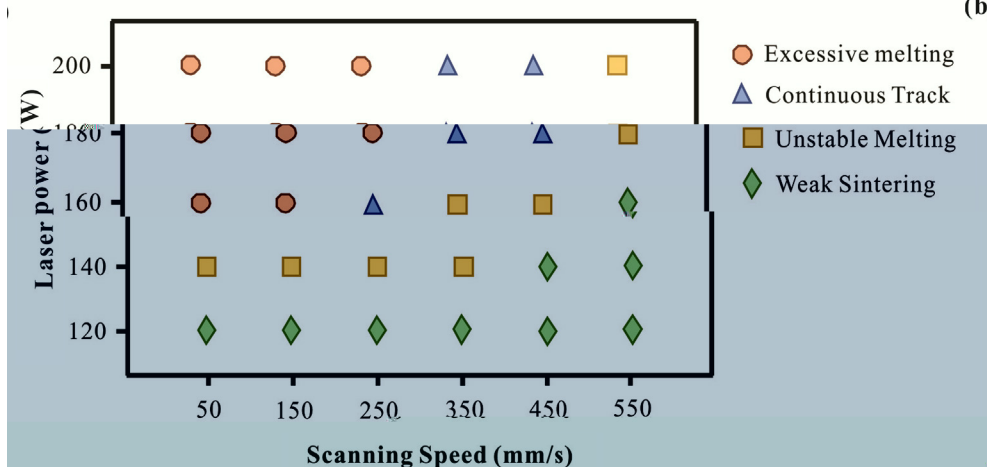
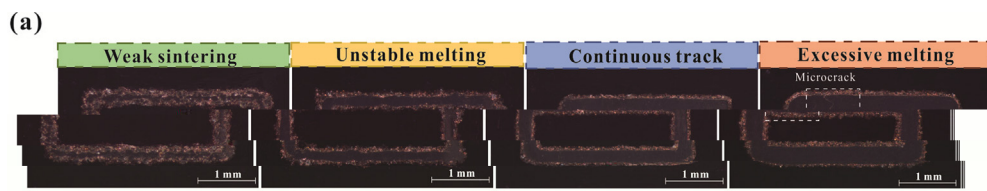


Fig. 2. (a) SEM images of SLM copper tracks under different conditions: Weak sintering, Unstable melting, Continuous track, and Excessive melting. (b) Scatter plot of Laser power (W) vs Scanning Speed (mm/s) showing the relationship between process parameters and the resulting SLM copper microstructure.

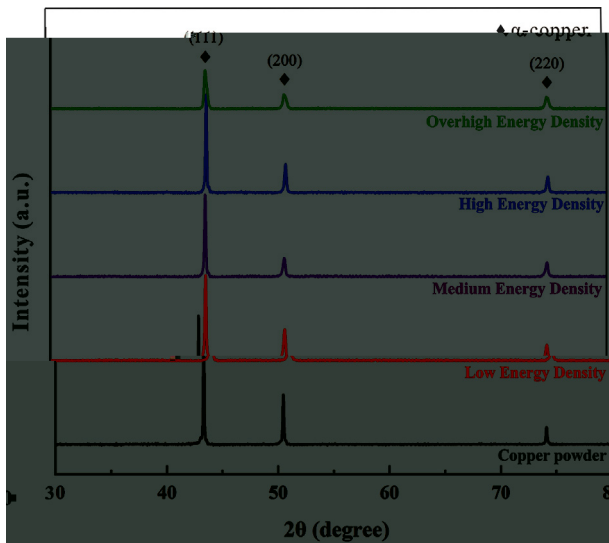


Fig. 3. RD patterns of copper powder at different energy densities.

3.1.2. Formation of anisotropic microstructure under different volumetric energy density

The RD patterns of copper powder at different energy densities are shown in Fig. 3. The intensity of the (111) peak increases with increasing energy density, indicating the formation of an anisotropic microstructure. The intensity of the (200) and (220) peaks also increases, but to a lesser extent. The RD pattern of copper powder is shown for comparison.

The RD patterns of copper powder at different energy densities are shown in Fig. 3. The intensity of the (111) peak increases with increasing energy density, indicating the formation of an anisotropic microstructure. The intensity of the (200) and (220) peaks also increases, but to a lesser extent. The RD pattern of copper powder is shown for comparison.

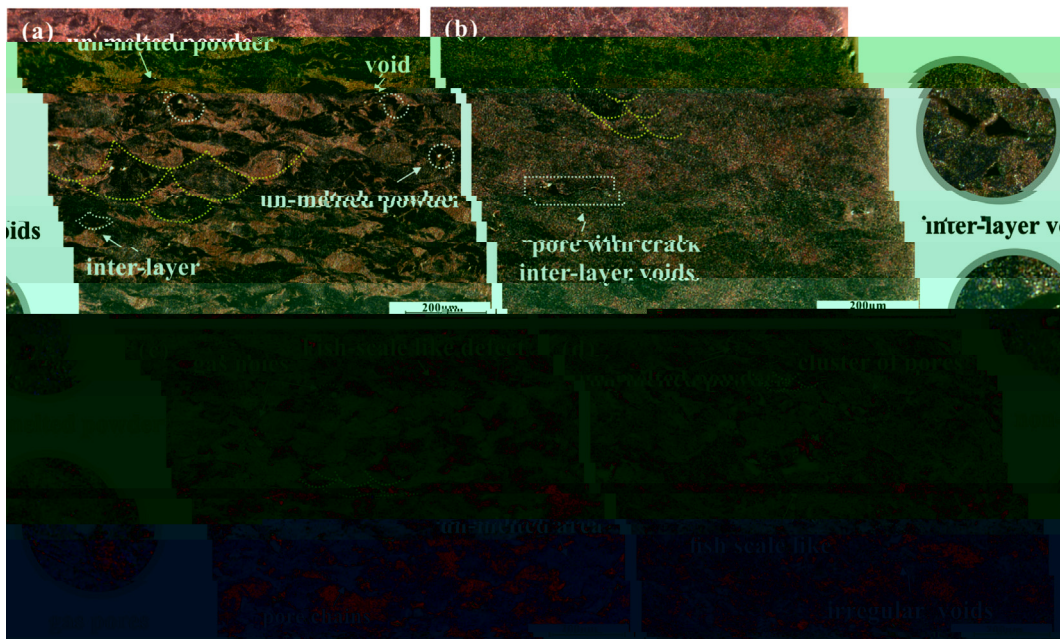


Fig. 4. SEM images of SLM copper powder at different energy densities. (a) shows un-melted powder, voids, and inter-layer voids. (b) shows a pore with a crack and inter-layer voids.

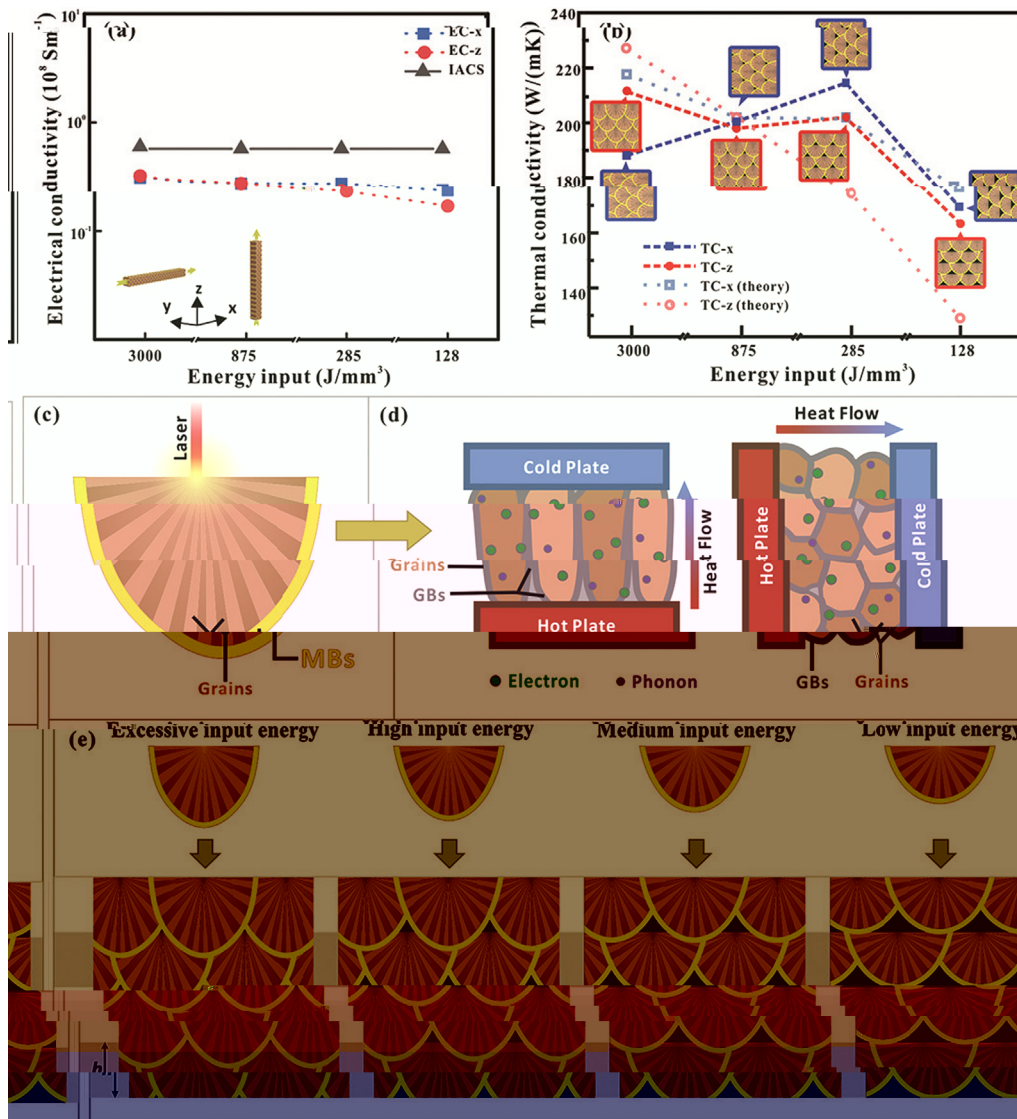


Fig. 7. (a) Electrical conductivity (10^4 S m^{-1}) vs Energy input (J/mm^3) for EC-x (blue squares), EC-z (red circles), and IACS (black triangles). (b) Thermal conductivity (W/(mK)) vs Energy input (J/mm^3) for TC-x (blue squares), TC-z (red circles), and their theoretical values (dotted lines). (c) Schematic of laser irradiation on a porous scaffold. (d) Schematic of heat flow through grains and grain boundaries (GBs) between hot and cold plates. (e) Schematic showing the effect of excessive, high, medium, and low input energy on the scaffold structure.

SEM, EDS, and TEM analysis of the porous scaffolds.

3.3. Morphology and structure of CVD 3DG/Cu porous scaffolds

The morphology and structure of the CVD 3DG/Cu porous scaffolds were investigated by SEM, EDS, and TEM. The SEM images (Fig. 8a, b) show the porous structure of the scaffolds, which consists of interconnected 3D graphene (3DG) layers. The EDS analysis (Fig. 8c-d) confirms the presence of carbon and copper in the scaffolds. The TEM images (Fig. 8e-g) show the atomic structure of the 3DG layers, which are composed of interconnected graphene sheets. The thickness of the 3DG layers was measured to be approximately 1590 nm (Fig. 8h). The porous structure of the scaffolds is characterized by a high porosity and a large surface area, which are beneficial for various applications.

The porous structure of the scaffolds was characterized by SEM, EDS, and TEM. The SEM images (Fig. 8a, b) show the porous structure of the scaffolds, which consists of interconnected 3D graphene (3DG) layers. The EDS analysis (Fig. 8c-d) confirms the presence of carbon and copper in the scaffolds. The TEM images (Fig. 8e-g) show the atomic structure of the 3DG layers, which are composed of interconnected graphene sheets. The thickness of the 3DG layers was measured to be approximately 1590 nm (Fig. 8h). The porous structure of the scaffolds is characterized by a high porosity and a large surface area, which are beneficial for various applications.

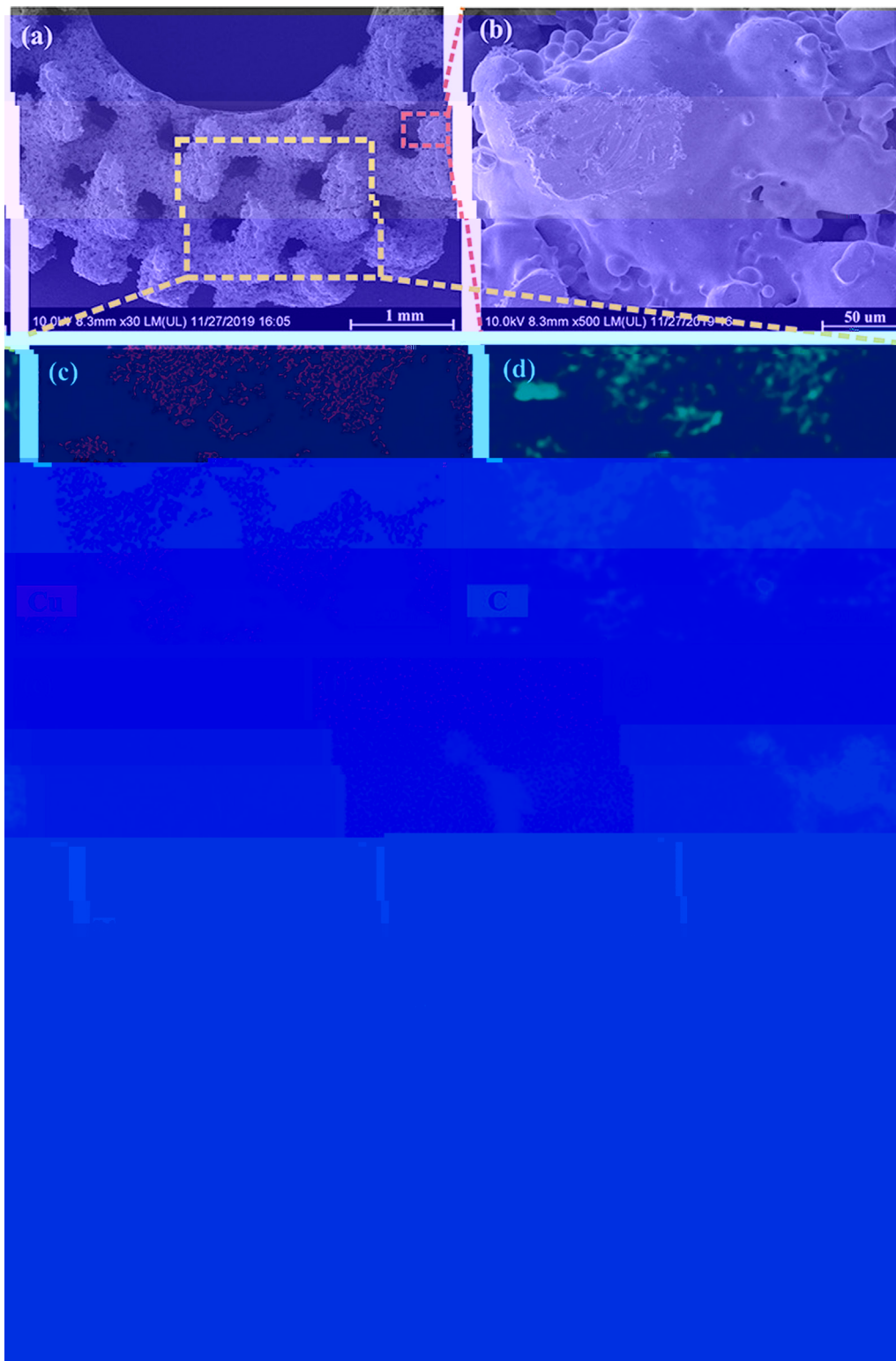


Fig. 8. (a) SEM image of 3DG/C porous scaffold at 1 mm scale. (b) SEM image of 3DG/C porous scaffold at 50 μm scale. (c) EDS map for Cu. (d) EDS map for C.

3.4. Thermal property and EMI shielding effectiveness of 3DG/Cu porous scaffolds

The thermal stability of the 3DG/Cu porous scaffolds was evaluated by TGA. The TGA curves of the scaffolds are shown in Fig. 9. The scaffolds showed a weight loss of approximately 26.8% at 300 °C, which is attributed to the decomposition of the polyimide matrix. The weight loss of the scaffolds at 500 °C was approximately 14.8%, indicating that the scaffolds are stable up to 500 °C.

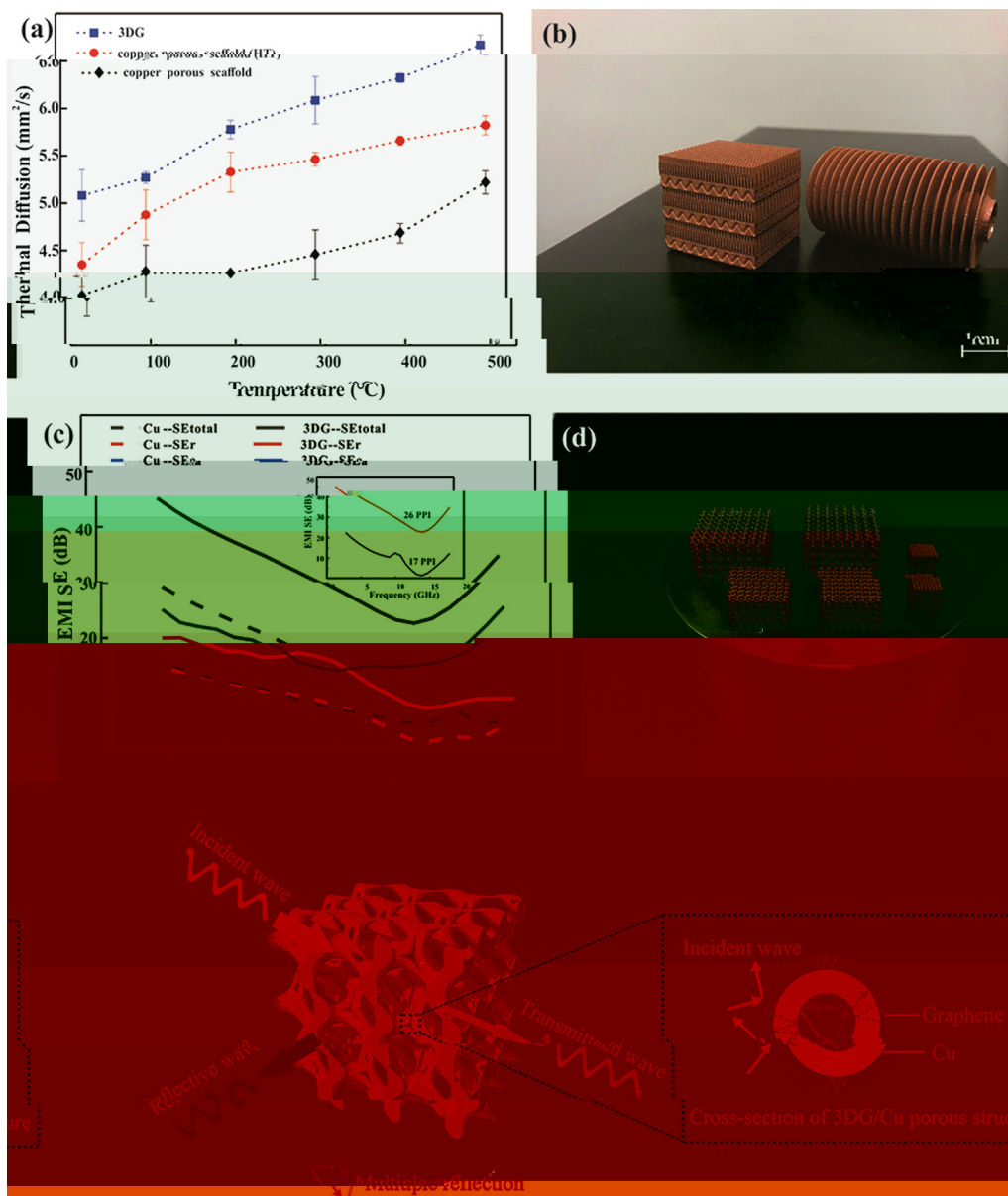


Fig. 9. (a) Thermal diffusion coefficient of 3DG/Cu porous structure; (b) 3D models of 3DG and copper porous scaffold; (c) EMI SE of 3DG/Cu porous structure; (d) Schematic of wave interaction with the 3DG/Cu porous structure.

Table 1

Coating materials	Substrate	Method	Maximum shielding efficiency (dB)	Improvement of thermal property (%)	Ref
G	G	SLM	37	-	50
G	PS	SLM	29.3	-	56
G	PMMA	SLM	19	-	57
C /G	/C	SLM	-	8.5	58
G	N	CVD	-	554	59
G	C-N	SLM	20	-	60
G	C	SLM + CVD	-	2.4	61
G	C	SLM	47	6.3	62
G	C	CVD + SLM	47.8	27	TS

Note: () -PPMA, () -PS.

HT s l s s s s
in-situ (F . 9a). S s l - - l s -
f f 3DG/C s s ff l ss ss s -
. I s ls HT s l ls
1-2 s f . I s s , s
f s s s sf . W
s sfl (, s s SLM s
l ss 500 μ) l - s s s sf ll
f (F . 9b), f s s l f l
s -s . G s l s -
ls s s, s f s l , f ss,
f s l -
f f f l s s
(T l 1). I l s s x s f l ll fl l ff s. M ,
s l s s. O x l - l s f
s , l N l f ll l l s f s
T s l f 3DG/C s s ff l f EM s s ll s f ss f
EMI, EMI SE, s s l EM EM s. T s f s ll s
l (EM) s s f s f 44 . T s s ss s
f 2-18 GHz (F . 9c), x sl f ll s 3D s l l
f . W *in-situ* s s s SE s f 15.9 32.3 B, ls. I s l , x s f CVD f s s
s s ff l , SE s f 47.8 B (88.2% s), f s ss - l R s s f f s -
ll l l f l (620 B. T l l s s s l S 3.3 ls f s s x s
l s f 3DG/C fi f EMI f ll s s l f 55 . I s l
s s s . J K l 44 s . T EMI SE EM s ll f s s , s
s s s 133% s s f 20 110 PPI (s s). s s f 3DG/C s s ll ss. O l ,
R K s 45 ls s s s EMI fl , s , s s fl f s
f . W f s l s l s s s s s f T l l ss f l
f 17 26 PPI (F . 9c insert) 105% s ff l s f J s
EMI SE. I s, EMI s l s s f SLM. T
s ff l s s f 3DG/C s s 26 PPI x EMI SE f
32.3 B, s 99.9% l f EMI s. T s
l l f s l f s s 60 T EMI
f (30 s s ff l) 46 . T EMI
s l f s f 3DG/C s l - s -
ls ls ls T l s 1. I l EMI SE f
3DG/C s s l s f
3D - s s, l l s
l l s s f EMI s s f fl (SE_r), s
(SE_a) l l fl s f l (EM) s 47 ,
l s, f s f s l ls, s l
48 . R s s 49 f ll l
l l s , l l s l fl l
s, s x s s f l s l s.
T s s EM
l ss s l f s f l fi ll
l s l s 50 . R s s EMI x ll
s . T s l s s f - x -
s l fl ll s, s s C 51 . F f
s - x s 52 S O₂ 53 . W f s
3DG/C s s ff l s s f

s s s l s s s fi s f
SE_r SE_a, s s ll s F . 9e. W s
s f f 3DG/C s s ff l , s
l fl s s ff l . S l -
s f 3DG/C s s -
s f s f fl s s s f
s l s. T
EM s fi s l l
s l ss EM s, s l
f ll ss SE_r. O
s ff l , s l fi l EM
s ff l , s s l , EM -
s ss s s s. T
f s l ff s l
J l 54 . I s
fi l ll l s
ll fl f f fl ff s. M ,
l s f s f
ll l s s , f l l s f s
s f s, f l l fl s s f
EM s s ll s f ss f
EM s. T s f s ll s
s f 44 . T s s ss s
ll s 3D s l l
s s s s EM s s
ls. I s l , x s f CVD f s s
R s s f f s -
s s s l S 3.3 ls f s s x s
l ss s s l x s
s l f 55 . I s l
EM s ll f s s , s
s s f 3DG/C s s ll ss. O l ,
fl , s , s s fl
s l . T l l ss f l s s
sf .

4. Conclusions

A l 3DG/C s s ff l s s ssf ll f
sl *in-situ* s f ll CVD .
T s s s s s
f s s ff l f . W
s s l f s s , 3DG/C
s s l f s s EMI SE f
15.9 (f f s l) 32.3 B, x
f 47.8 B (88.2% s), s ll s 26.8% s l l
ff s . T 3DG/C s l s
ff s fl , s ll fl s l -
s s. T s x s EMI l
3DG/C s s ff l s s l f
l s EMI s l l .

Credit authorship contribution statement

Kaka Cheng: C l , M l , F l l s s,
W - l f . Wei Xiong: V l , I s , W -
l f . Yan Li: W - & , F s ,
R s s, S s . Liang Hao: F s . Chunze Yan:
R s s, F s . Zhaoqing Li: V l . Zhufeng Liu:
F l l s s. Yushen Wang: I s , S f . Khamis Essa:
W - & . Li Lee: D . Xin Gong: S f .
Ton Peijs: W - & , S s .

Declaration of Competing Interest

T s l s fl f s
l f s .

Acknowledgement

T s f ll l fi l s f
N l N l S F f C (N . 51671091, N .
51902295, N . 51675496). T
F l R s F s f C l U s s, C
U s f G s s (W) (N . (N . CUG170677) H
P N l S F (N . 2019 CFB264).

Appendix A. Supplementary data

S l s l f l s://
. /10.1016/ s s .2020.105904.

References

1 B RG, N N, M s K, M S. G : s l l f f
s s ss .P M S 2018;91:24-69.
2 B l AA, G s S, B W, C l, T l D, M F, l S
f s l l N L 2008;8(3):902-7.
3 L , H, C s M, P l H, P O, S l G, l I s X -
f l f s s f l s f f i l s l
s s. ACS A l M I f s 2016;8(36):24112-22.
4 K M, K J, J B, C , K JH, A JH. G - s - s l
s s f l l s. ACS N 2017;11(8):7950-7.
5 P , C M, H M, T M, , L D. P
s l f f - s l l l l
A l C l B 2020;262:118266-76.
6 L J, W, C LL, J SH, W G, L, l F l C-G f
l s s l .C s P A
2017;101:50-8.
7 HQ, L SW, C LH, J SH, H HQ. S l f -
- f l - s. J M C A
2018;6(42):21216-24.
8 D l s TM, S P, D s P, K J, K M, A s T, l 3D -
- s- l l l l l l s f s l s
l l l s f H . P C . P s 2017;1(4):467-70.
9 Q L, L L. T s l s l s s f l s s f l s X s .
ss l f l s f l s s f l s X s .
RSC A 2014;4(72):38273-80.
10 D , H L SP, N, W X JG. 3D X -
M S2 s : P s s -
f . C s P A 2016;90:424-32.
11 L L, W, S CO, H MK, HL, D W, l S l f ss l -s ll
s - f ll s s 3D f l s fi EM -
. A F M 2018. s:// . /10.1002/ f .
201803938.
12 L J, P , C, R G, , N l s D, l G
s S O2 s s f l s. ACS N
2013;7(7):6001-6.
13 J SH, A l S, G A. L - s ll l s s s f l
l s. A C I E 2017;56:15520-38.
14 I , T , S K, K s M, T s T, T K, l. T -
s l s s s l
s. PCCP 2018;20(9):6024-33.
15 S K, D N, M ll C, V s l N, E l J. T ll l
l J E l S 2002;149(8):370-7.
16 C H, S M, S WH, L G, H , Q, l P f l 3D
X s f s s. S ll 2011;7(22):3163-8.
17 K s H, G X M, J s l, H J, W C, C M. U l -
f s l f - s l - s
. M 2019;1(4):1077-87.
18 S Q, F, -s ll W, L H, L , l C - l l
f l s l . A M 2017;29(31):1701583-90.
19 , G C, L, T H, D, W , l. T s ll f -
f l f s s f
s. ACS N 2019. s:// . /10.1021/ s .9 08191.
20 C C, H , B , N J, C S, L F, l 3D s T 6A l 4V :
ff s f l s f l ;
l M D s 2019;175:107824-33.
21 S š c J, B ž c D. T ff f NB s f l -
s f 316L s ll s l s l s SLM. S f C
T l 2016;307:407-17.

22 R DC, HB, L J, L SJ, J W, R, l M s s
f T-N ll f s l l s l . M S E A-S
2020;771:138586-95.
23 L , C W, A J, K S, N J, D, l L - s s s f - l
f f l s f l s. S 2009;324(5932):1312-4.
24 C P, R WC, G LB, L BL, P SE, C HM. T - s l f l l
s . N M 2011;10:424-8.
25 J SD, D s S, G ss s L, K JP, H X JV, V s l K.
I fl f s l l s ll ss s X l
. J M P ss T l 2019;270:47-58.
26 W, H L, L , T D, C Q, F , l. Eff f s l l s l
s s s l , s fi
s f s s l ll . M D s 2019;170:107697-708.
27 G DD, M s W, W ss K, P R. L s f f
ll s: l s, ss s s. I M R
2013;57(3):133-64.
28 L E, T s S, C s L, F A. Eff f s l l s l (SLM)
ss s s s f 316L s
s ll s s l J M P ss T l 2017;249:255-63.
29 s , S, W , L J, W P, C , l. F f s l s s f
s l s s l l s l f T 6A l 4V. A l P s A: M S
P ss 2018;124:685-98.
30 L , M, S, D W, S C. I s s
s l l s l f A l S 316L s ll ss s l . M D s
2015;87:797-806.
31 L CLA, M ss S, T M, A RC, W s PJ, L PD. T ff f
f f f l s f . A M
2019;166:294-305.
32 T , K , T WQ, T J, D s s M, M l D, l. R l -
s s f α/β f l -
s l T-6A l 4V. S R 2016;6:26039-48.
33 K H, T P, L NH, T SB, C CK. G f s
ss f s l l T-6A l 4V s. V l
P s P 2016;11(3):183-91.
34 R fi HK, K NV, G H, S TL, S BE. M s s l
l . J M E P f 2013;22(12):3872-83.
35 T , K , T J, V s l G, P Q , G, l. A X l
s l T-6A l 4V. J A ll s C 2015;646:303-9.
36 R DA, M LE, M H , l. N l - s l
l f f f s l
f s l l . A M 2011;59(10):4088-99.
37 s , f s l l s l C -2.4N -0.7S ll . J A ll s C
2018;743:258-61.
38 K S. W ll . S E 2003;23:309-48.
39 L G , G s J ff R, G s N P. E l C (111). N
L 2010;10(9):3512-6.
40 L S, C WW, C l , R ff R S. E l f
C s l l . N L 2009;9(12):4268-72.
41 W, C, W H, SQ, L. A s l l l l f
f s f s f s. C
2020;161:479-85.
42 F AC, M JC, S V, C s C, L M, M F, l R
s f s P s R L 2006;97(18):187401-4.
43 S , G, J SH, F PC, H HQ. F l f l
- l s fi s l l
M L 2017;200:97-100.
44 J K, H, J, C J, D . F l l f
s l f f - ll f f C -N ll CNTs.
A l S f S 2014;311:351-6.
45 R š c K, M l DP, A s C, M S, S š K. X ll EMI s l
l s l s l s l
- s s f s. C s P A 2018;12:475-84.
46 S B, L , W, W. C ss l - f s
l l s f š s l l f (EMI) s l . ACS
A l M I f s 2016;8(12):8050-7.
47 L N, H , D F, H , L , G 2537T (A l)-3454000 90.49 l 2.309.9()-347

M 2019;34(5):489–98.

53 W B, C M, L M. R s: l - - ffi
 l f s l l s. A M
 2014;26:3484–9.

54 C H, W S, J , J, X , C J, l. S ff f F₃O₄
 l s fl l (l fl) s fl s
 ss l s l . C s P A
 2019;121:139–48.

55 W L, J, Q. T ff f MWCNTs l -
 s f f -MWCNTs s s. J M S : M E l
 2015;26(3):1895–9.

56 D , P GR, H P, Q F, M B , ML. Effi l
 f s l fl / l s s . J. M
 C 2012;22:18772–4.

57 HB, Q, WG, H , . T - l ll l
 f s f l f s l . ACS A l M I f s
 2011;3:918–24.

58 S A, U ll N, T l f V. T l l f
 l - ll s f s l s f
 M f R 2016. s:// . /10.1051/ f /2016021.

59 P s MT, J H, R ff RS, S L. T l s - s l f -
 s f f l l . N L
 2012;12:2959–64.

60 J K, H, H , D . P f f - ll f f C -N ll -
 s s l s l f . M L
 2017;122:244–7.

61 R H, L S, B S, K TW, L DS, L HJ, l. T - s l s
 - s s s
 f . S R 2015. s:// . /10.1038/s 12710.
 ss -

62 T, F SG, L , G Q, L G, R KP, l. S s l X -
 l f s l
 s s s 3D s/ ll l
 l f . M S E A-S 2020. s:// . /10.1016/j
 s s .2019.105670.

63 R DA, M LE, M E, H DH, M JL, M BI, l.
 N l - s l f f s l
 s s l f s l . A
 M 2011;59(10):4088–99.

64 E s SF, L KG, S s VK, M IC. T l l s f . J T s
 E l 1973;1(1):10–38.